Clim. Past Discuss., 11, 307–343, 2015
www.clim-past-discuss.net/11/307/2015/
doi:10.5194/cpd-11-307-2015

Climate of the Past Discussions
Open Access

A regional climate palaeosimulation for Europe in the period 1501–1990 – Part II: Comparison with gridded reconstructions

J. J. Gómez-Navarro[1], O. Bothe[2], S. Wagner[2], E. Zorita[2], J. P. Werner[3], J. Luterbacher[4], C. C. Raible[1], and J. P. Montávez[5]

[1]Climate and Environmental Physics, Physics Institute and Oeschger Centre for Climate Change Research, University of Bern, Switzerland
[2]Institute of Coastal Research, Helmholtz-Zentrum Geesthacht, Geesthacht, Germany
[3]Department of Earth Science and Bjerknes Centre for Climate Research, University of Bergen, Bergen, Norway
[4]Department of Geography, Climatology, Climate Dynamics and Climate Change, Justus Liebig University of Giessen, Giessen, Germany
[5]Department of Physics, University of Murcia, Murcia, Spain

Received: 13 January 2015 – Accepted: 26 January 2015 – Published: 13 February 2015

Correspondence to: J. J. Gómez-Navarro (gomez@climate.unibe.ch)

Published by Copernicus Publications on behalf of the European Geosciences Union.

Abstract

This study jointly analyses gridded European winter and summer surface air temperature (SAT) and precipitation reconstructions and a regional climate simulation over the period 1501–1990. The European area is analysed separately for nine sub-areas. In their spatial structure, an overall good agreement is found between the reconstructed and simulated climate variability across different areas of Europe, supporting a consistency of both products and the proper calibration of the reconstructions. Still, systematic biases appear between both datasets that can be explained by a priori known deficiencies in the simulation. However, simulations and reconstructions largely differ in their estimates of the temporal evolution of past climate for European sub-regions. In particular, the simulated anomalies during the Maunder and Dalton minima show stronger response to changes in the external forcings than recorded in the reconstructions. This disagreement is to some extent expected given the prominent role of internal variability in the evolution of regional temperature and precipitation. However, the inability of the model to reproduce a warm period similar to that recorded around 1740 in winter reconstructions is indicative of fundamental limitations in the simulation that preclude reproducing exceptionally anomalous conditions. Despite these limitations, the simulated climate is a physically consistent dataset, which can be used as a benchmark to analyse the consistency and limitations of gridded reconstructions of different variables. Comparison of the main variability modes of SAT and precipitation indicates that reconstructions present too simplistic character of (natural) variability modes, especially for precipitation. This can be explained through the linear statistical techniques used for reconstruction. The analysis of the co-variability among variables shows that the simulation captures reasonable well the canonical co-variability, whereas independent reconstructions show unrealistically low correlations. Thus, the analysis points to a lack of dynamic consistency that reduces the confidence for subcontinental European reconstructions.

CPD
11, 307–343, 2015

1 Introduction

Confidence in projections of future climate change is supported by a better understanding of current and past climate changes and by the assessment of the skill of climate models in replicating past and present climate variations (Schmidt et al., 2014). In turn, evidence about the climate in pre-industrial times stems from various sources such as instrumental observations, documentary evidence, environmental proxy-archives or climate simulations. Given this variety, gaining reliable insight in past climate variability requires climatological, statistical and dynamical consistency across these different sources, especially between reconstructions and simulations. However numerous uncertainties, outlined below, affect the assessment of past climate variability.

Disagreements between simulations and reconstructions may be caused by deficiencies in reconstruction methods (e.g. Tingley et al., 2012), by model limitations that reflect the inadequate spatial resolution and missing physical processes (Gómez-Navarro et al., 2011, 2013) or both. Beyond these methodological shortcomings, both data sources ultimately rely on inferences from environmental archives, since simulations require to some extent input from reconstructions of past forcing data too. Environmental proxies (Evans et al., 2013) record influences of various environmental factors and, in turn, palaeo-observations do not necessarily perfectly reflect one particular environmental variable (e.g. Franke et al., 2013). Rather, they usually explain only part of the variability of the variable of interest.

In addition to shortcomings in the datasets, internal variability may become dominant compared to externally forced signals in the variable of interest (e.g. temperature or precipitation), especially at regional scale (Gómez-Navarro et al., 2012). This implies that a single model simulation represents only one possible realization, among infinite many, of a possible past climate evolution constrained by initial and boundary conditions and the presence of unforced natural internal climate variability. Thus, a perfect agreement with reconstructions cannot be expected at local scales. At larger scales the random internal variability is averaged out. In addition internal modes of

CPD
11, 307–343, 2015

climate variability may respond to external forcing events like large tropical volcanic eruptions (Yoshimori et al., 2005; Zanchettin et al., 2012) or variations in components of changes in solar activity (Shindell et al., 2001). However, especially the influence of low-frequency solar activity changes on climate and climate variability, is still under discussion (Gómez-Navarro and Zorita, 2013; Anet et al., 2013, 2014; Raible et al., 2014). Environmental archives integrate these internal variations, and while climate simulations cannot be expected to replicate the exact unforced variations, they ideally should be capable of replicating the forced variability (if they include the relevant processes).

Attempts to reconcile climate simulations and reconstructions are further hampered by fundamental differences in the characteristics of the information they provide. Simulations and reconstructions represent data on different spatial and temporal scales. Simulations provide information with high temporal resolution and spatially averaged to the grid-cell size. Reconstructions are based on archives which are affected by local climate conditions. Additionally, the specific relation between local and large scale environmental factors is only partially constrained (Kim et al., 1984). Various approaches exist for combining the information obtained from reconstructions and simulations. Among them are proxy-forward models (Phipps et al., 2013; Evans et al., 2013), data-assimilation (Goosse et al., 2006, 2012; Widmann et al., 2010) and proxy surrogate reconstructions i.e. analog methods (Franke et al., 2010; Luterbacher et al., 2010). In addition to these techniques, dynamical and statistical down- and upscaling methods are currently introduced (Gómez-Navarro et al., 2011, 2013; Wagner et al., 2012; Eden et al., 2014).

The basis of dynamical downscaling includes the implementation of a Regional Climate Model (RCM), driven at its boundaries by a Global Circulation Model (GCM). This allows spatially highly resolved climate simulations over limited areas, consistent with the driving model. This downscaling approach provides the potential to bridge the spatial scale gap between simulated and reconstructed estimates of past climate variability. Besides refining the spatial resolution of the model dynamics, the more detailed

CPD
11, 307–343, 2015

orography of regional simulations also allows an improved representation of the regional scale boundary conditions. This approach has been successfully applied over the Iberian Peninsula (Gómez-Navarro et al., 2011) or the Baltic Sea (Schimanke et al., 2012). However, the relatively low number of available regional palaeoclimate simulations is a fundamental restriction. Recently, Gómez-Navarro et al. (2013) have shown how a high resolution regional climate simulation with the RCM MM5 is able to improve the performance of its driving GCM when compared to 20th century observations over Europe.

Despite the limitations of climate models, a remarkable benefit relates to their dynamically consistent estimates for different variables, because the evolution of the climate within the model is produced by the application of well-known physical conservation laws. This allows us to assess, through a suitable comparison between reconstructed and simulated climates, to what extent the reconstructions provide dynamically consistent estimates of past climate variability. Likewise it permits to evaluate the consistency of climate reconstructions for different variables, their spatio-temporal distributions and their main variability modes.

Here, we extend the previous assessment of Gómez-Navarro et al. (2013) by evaluating the level of agreement between a regional simulation over Europe for the period 1501–1990 and available reconstructions of seasonal air temperature and precipitation. We focus our analysis on regions where Gómez-Navarro et al. (2013) found that the regional model provides added value beyond the skillful spatial scales of the global climate model. This way we increase our confidence not only in potential agreement between simulations and reconstructions, but also in the conclusions we can draw from potential disagreements. That is, we do not benchmark the simulation against the reconstruction, instead we jointly analyse both uncertain estimates with the aim of increasing our understanding of past seasonal climate changes in Europe.

The manuscript is organized as follows: in the following section we introduce the observations, simulation and reconstructions used for analysis, including a short overview of the methods. In Sect. 3 we discuss the past climate evolution in terms of seasonal

CPD
11, 307–343, 2015

surface air temperature and precipitation variability present in the data for a number of European sub-regions. We analyse the evolution of probability density functions of precipitation and temperature. In Sect. 4 we turn our attention from the temporal agreement towards the variability modes; we first compare the dominant reconstructed and simulated variability modes (Sect. 4.1) for temperature and precipitation. Then, we investigate the consistency between these variables and sea level pressure in terms of canonical correlation. A discussion and subsequent concluding remarks close the study.

2 Data and methods

2.1 Climate simulations

Our analysis uses the output of a high-resolution climate simulation carried out with a RCM over the Europe for the period 1501–1990. The RCM consists of a climatic version of the meteorological regional model MM5. This simulation is driven at its boundaries by the Global Circulation Model (GCM) ECHO-G. The horizontal model resolution is 45 km and its domain covers Europe almost entirely (see Fig. 1). This nesting setup is referred hereinafter as MM5-ECHO-G. Both models are driven by identical reconstructions of several external forcings to avoid physical inconsistencies: greenhouse gases, Total Solar Irradiance (TSI) and the radiative effect of tropical volcanic events. This simulation is described in detail by Gómez-Navarro et al. (2013), including a discussion of the skill of the model MM5-ECHO-G in reproducing the European climate against observational precipitation and temperature gridded datasets. Results of this validation indicate an added value with respect to the driving GCM. However, there are still deviations between the regional simulation and the observations. Prominent problems relate to the divergent 20th century temperature trends. Gómez-Navarro et al. (2013) argued that this could originate from missing anthropogenic aerosol forcing in the simulation, which is an important factor with a potential net cooling effect, especially in the second

CPD
11, 307–343, 2015

half of the 20th century (Andreae et al., 2005). Furthermore, the driving simulation with ECHO-G simulates a strong positive trend in the North Atlantic Oscillation (NAO) index under anthropogenic forcing, which is absent in the observations. This leads to a negative trend in winter precipitation in southern Europe and a positive trend in near surface air temperature (SAT) over Northern Europe. These disagreements have two potential and complementary explanations. On the one hand, the missing aerosol forcing could explain part of the circulation trend (e.g. Booth et al., 2012). On the other hand, much of the NAO variability is related to internal variability (Gómez-Navarro and Zorita, 2013), so the disagreement between model and observations could a priori expected in the NAO index, regardless of the forcing employed.

2.2 Observational datasets

This analysis employs various observational datasets to obtain the main variability modes of SAT, precipitation and Sea Level Pressure (SLP). These are compared to the corresponding results obtained for the model and the statistical reconstructions. SAT and precipitation are taken from the monthly data set developed by the Climate Research Unit (CRU) at the University of East Anglia (Harris et al., 2014). This is a global gridded product over land areas with a spatial resolution of $0.5^{\circ} \times 0.5^{\circ}$, including several climatic variables for the period 1901–2005. In this comparison exercise only temperature and precipitation series up to 1990 are considered, since this is the overlap period between observations and simulation. The data are bi-linearly interpolated onto the MM5 grid to provide a suitable basis for comparison. To keep consistency with reconstructions, only land points are considered for the comparison.

The SLP field consists of monthly means of this variable extracted from the NCEP reanalysis for the period 1948–1990 (Kalnay et al., 1996). This dataset has a spatial resolution of $2.5^{\circ} \times 2.5^{\circ}$, slightly higher than ECHO-G, and has been used on its original grid without any further spatial interpolation.

CPD
11, 307–343, 2015

2.3 Gridded reconstructions

We use climate reconstructions for three variables, winter and summer SAT, precipitation and SLP. In particular we use the gridded data sets by Luterbacher et al. (2004, 2007) for SAT and Pauling et al. (2006) for precipitation. Both data sets consist of seasonal series on a 0.5° × 0.5° regular grid over land areas of Europe. Similar to observations, these datasets were interpolated onto the MM5 grid prior to analysis. These reconstructions are based on a large variety of long instrumental series, indices from historical documentary evidence and natural proxies (see Luterbacher et al., 2004, 2007; Pauling et al., 2006, for details). The basis for the reconstruction is related to the use of linear methods (i.e. principal component regression). Despite the underlying assumptions, e.g. the stationarity of the relationship between the proxy and the climatic variable, the method is able to provide gridded fields for both, temperature and precipitation. Luterbacher et al. (2004, 2007) and Pauling et al. (2006) critically addressed the uncertainties and skills of their reconstructions, especially in the early period of the 16th and 17th century, when less records and only those with lower quality are available. Also Pauling et al. (2006) provide performance maps for their precipitation reconstruction for the reduction of error (RE) of the reconstruction. This allowed a rigorous assessment of the spatial pattern of skill of the reconstruction. An important characteristic of the reconstructed precipitation in contrast to reconstructed temperature relates to the large spatial heterogeneity caused by a considerably shorter spatial de-correlation distance of precipitation. This characteristic becomes critical when attempting to reconstruct hydrological fields from a sparse network of proxy data (Gómez-Navarro et al., 2014).

The SLP reconstruction has been selected after certain criteria. Our analysis avoids using the Luterbacher et al. (2002) reconstructions for SLP, because it uses some of the proxies employed in the SAT and precipitation reconstructions. Thus, the use of this dataset would preclude the evaluation of the dynamical consistency among reconstructions without introducing circular arguments. Hence, we use an entirely indepen-

CPD
11, 307–343, 2015

dent SLP reconstruction. In particular, we use the SLP reconstruction by Küttel et al. (2010), which is based only on station pressure data and ship logbook information. This dataset has a resolution of 5° × 5° and spans the period 1750–1990.

2.4 Framework of the joint analysis of simulated and reconstructed climate

As discussed in the introduction, besides model and reconstruction errors, internal variability prevents perfect agreement between the temporal evolution of the simulated and reconstructed climate variables (Gómez-Navarro et al., 2012). A simple way to partially ameliorate this problem is low-pass filtering the climate series. The underlying argument is that the ratio of forced to internal variability is higher at lower frequencies. Since the degree of required filtering is unknown we simply apply a 31 years running mean using a Hamming window.

In the following we compare the temporal evolution of temperature and precipitation simulated by MM5-ECHO-G with the reconstruction of Luterbacher et al. (2004, 2007) and Pauling et al. (2006), respectively, in nine European sub-domains (Fig. 1). We restrict the analysis on the period prior to 1900 to prevent an overlap from the calibration period. As the reconstructions are calibrated using the observational or reanalysis datasets, they should basically agree with the observations used in (Gómez-Navarro et al., 2013) for validation purposes. The authors highlighted the general overestimation of temperature trends in the simulation during this period, which is strongest for winter in northern Europe. Similarly, precipitation trends of observations and the simulation during the 20th century are often not consistent. We note the contrast between observed wetter conditions and simulated drying in southern Europe in winter. Gómez-Navarro et al. (2013) also found that the regional simulation improved the representation of the observed climatology in the European sub-domains of Scandinavia and the Baltic Sea (SCA), the British Isles (BRI), the Iberian Peninsula (IBE), the Alps (ALP), the Balkan Peninsula (BAL), the Carpathian region (CAR) and Turkey (TUR) relative to the global simulation, whereas the representation did not improve much for Central Europe and Eastern Europe. Therefore we restrict to the five regions with skill.

CPD
11, 307–343, 2015

However, a simple comparison of the time series might be misleading given the presence of internal variability in the simulation. For this reason, we additionally use Empirical Orthogonal Functions (EOF) analysis to identify the main variability patterns of mean seasonal SAT and precipitation. These patterns are not critically dependent on the precise temporal evolution within each dataset. Thus, they facilitate the comparison of the climate variability reproduced by the model and the reconstructions. Similarly, Canonical Correlation Analysis (CCA) helps to identify co-variability between climate variables in a linear sense, which gives a hint about potential underlying physical mechanisms. Thus, this statistical tool allows us to assess the dynamical consistency among different reconstructions. The two aforementioned techniques are widely used in climate research, therefore we provide only a brief introduction here (the reader is referred to von Storch and Zwiers (2007) for a comprehensive overview).

The basic philosophy of EOF analyses relates to decomposing the spatial (anomaly) fields of the climate variable under consideration into patterns representing most part of its variance. An important characteristic of the resulting patterns (denoted as EOFs) and their corresponding time-dependent amplitudes relates to the fact that they are mutually orthogonal in the space and time. From a statistical point of view this characteristic is often of interest, but from a more physical point of view the interpretation of the EOF pattern may be complicated because the real world processes and patterns are not necessarily orthogonal. i.e. uncorrelated. Therefore, the physical interpretation of EOFs has to be performed with caution, especially when consecutive EOFs explain similar amount of variance and higher indexed EOFs.

CCA is related to the former technique. It also decomposes the original variable in a number of components or patterns. However, in this case the aim is to identify pairs of patterns in two variables whose temporal component in the original series exhibits a maximal temporal correlation. Similarly to EOFs, the resulting CCA pairs of time series are ranked according to their mutual correlation, although an important difference with EOF is that in this technique the canonical pairs do not form an orthogonal decomposition of the original space. Instead, the CCA time series corresponding to

CPD
11, 307–343, 2015

consecutive pairs are uncorrelated in time. Often the most physical meaningful information is spanned by the leading CCA patterns, although the associated patterns may not explain the largest amount of variance. An advantage of CCA for our purposes is that it helps disentangling the most important (canonical) relationships between climate variables, either in the observations, the reconstructions or simulations. Hence, from a physical point of view the leading patterns should show similar characteristics when the mechanisms leading to the relationships between the climate fields are controlled by the same processes. Conversely, deviations from this behaviour are indicative of physical inconsistencies among variables.

3 Temporal agreement of regional series and climatologies

3.1 Regional time series

The bold red lines in Fig. 2 show the evolution of the averaged SAT (estimated through the median value within each subregion) in the ECHO-G-MM5 model and the Luterbacher et al. (2004, 2007) reconstruction for winter and summer. As outlined in the former section, the series are low-pass filtered with a 31 year (Hamming low-pass filter) to emphasise the low-frequency variability. Both the reconstruction and simulation generally agree in their low-frequency evolution over northern Europe. Over southern Europe no clear-cut similarities can be seen (note the different scales in different areas and seasons). Similarly, variability is larger in winter than in summer in both data sets. This agreement is directly related to the skill of the model setup to reproduce the general climatic features of the European climate (Gómez-Navarro et al., 2013), and the fact that the reconstructions are calibrated against observational records over the 20th century. Hence, this agreement is directly linked to the consistency of both data sources and their ability to reproduce the observed climate during the 20th century. The most prominent bias is found with the generally lower summer temperatures in most sub-domains in the simulation compared to the reconstruction. The opposite behaviour

CPD
11, 307–343, 2015

is found in winter, with most of western and northern European areas exhibiting warm biases (Fig. 2). This is in good agreement with the biases discussed by Gómez-Navarro et al. (2013) in the context of the comparison of model and observations during the 20th century. Hence, the disagreement can be attributed to systematic biases within the simulation, which in turn are related to a too zonal simulated atmospheric circulation of the driving GCM Gómez-Navarro et al. (2013).

Regarding the centennial to decadal evolution, the simulation and reconstruction generally agree until 1700. There are anomalous episodes which appear to be synchronised between different regions (Fig. 2). This can be seen in the reconstructions and the simulation independently, and is indicative of prominent anomalies taking place at large spatial scales. However, these episodes are not synchronised across both data sets, indicating that these decadal variations might be unrelated to variations of external forcings.

Since the early 19th century the simulated summer and winter temperatures show a clear warming trend across all regions. The trend of the temperature reconstructions trends start later, are generally lower and/or restricted to one of the two seasons. Thus, regional decadal anomalies of simulated and reconstructed data diverge for most regions over the past approximately 200 years. However, disagreement at decadal scales increases in some regions already in the early 18th century. While IBE, BRI, ALP, BAL and TUR reconstructed and simulated series start to diverge in the early or the mid-19th century, CAR and SCA show pronounced anomalies in the 18th century which lead to large simulation-reconstruction deviations. This is also seen in the central and eastern European domains. Overall, there are no statistically significant correlations between the filtered series of reconstructed and the simulated SAT, (taking into account the presence of serial autocorrelation in the filtered time series).

A remarkable feature in reconstructed temperature evolution is the extremely warm period in winter in areas such as SCA or also EEU, and less notably in ALP or CAR, during the first half of the 18th century. This anomalous period has been discussed in detail by Jones and Briffa (2006) and Zorita et al. (2010). This period is present

CPD
11, 307–343, 2015

across independent reconstructions, and therefore a certain level of confidence exists that it was indeed a real phenomenon. However, this anomaly is not reproduced in the simulation, neither in this nor any other period prior to the late 20th century. Generally, the simulated summer temperature agree better with reconstructions than for the winter season. The inability of the model to reproduce such noticeable anomaly has several implications: on the one hand, internal variability could be responsible for such anomalous events, rendering an agreement very unlikely or virtually impossible. On the other hand, the fact that such an anomalous period is not reproduced in any other period of the simulation points towards fundamental limitations in the simulation that unrealistically restrict the spectrum of possible simulated extreme events (see also the discussions in Wetter et al., 2014).

The time series of seasonal precipitation are shown in Fig. 3. Gómez-Navarro et al. (2013) described how the RCM more clearly improves the representation of seasonal precipitation than of temperature relative to the driving GCM. This is mainly due to the fact that precipitation processes are more notably influenced by orographic features, which are better resolved in the RCM. Similar to SAT, there are noticeable biases that can be explained with model deficiencies. For example, the model tends to overestimate winter precipitation in central and northern Europe in the observational period since 1905 (Gómez-Navarro et al., 2013), which generates a wet bias in SCA, CEU or EEU. It is noteworthy that biases are not so much prominent in summer, as is also the case when the model is compared to observations for the 20th century (Gómez-Navarro et al., 2013). Independently from the biases, the agreement between simulation and reconstruction is expected to be lower for this variable due to the larger imprint of internal and small-scale variability on precipitation (Gómez-Navarro et al., 2012, 2014).

A comparison between seasonal reconstructed and simulated precipitation shows less variability in northern than in southern areas (again note the different scales). The temporal variability appears to be particularly large in areas of complex orography such as ALP, TUR or IBE. Both data sets show strong low-frequency variations in most

CPD
11, 307–343, 2015

regions with pronounced dry and wet episodes over the period 1501–1900. However, these are neither synchronised between both data sets nor for the two seasons (Fig. 3). Variability also appears to change over time. For instance, simulated winter variability increases in TUR whereas reconstructed summer variability weakens in CAR.

The most prominent features and discrepancies between reconstructions and the simulation sorted by century are: in the early 16th century, CAR and ALP suggest prominent summer dryness, which is absent in the other series. Reconstructions further suggest wet winters in BRI in the 16th century. There are hints of coherence between reconstructed and simulated summer ALP precipitation. Reconstructed summer precipitation in the 17th century indicates very wet conditions for CAR, BAL and ALP while BRI summers appear to have been dry. Anomalous dryness is also seen in the early 18th century in summer in CAR, TUR, BAL and ALP reconstructions while summers were wet in BRI and SCA during that period. Winter wetness in the 19th century is prominent in many regions in the simulation (Fig. 3).

A regional peculiarity is a pronounced alternation between drier and wetter conditions with diminishing amplitude and shortening period between 1501 and 1800 in reconstructed CAR summer precipitation. Variations in TUR winter precipitation are very large in the simulation but rather low in the reconstruction. Iberian winter precipitation shows an apparent anti-phase between simulation and reconstruction.

In summary, we see no clear forcing imprint in either data set and no general congruence between the simulation and reconstructions. Pronounced anomalous periods are evident in reconstructed winter temperature in the early 18th century and in reconstructed 17th and 18th summer precipitation which are absent in the simulation.

3.2 Evolution of climatological probability distributions (PDFs)

The nine regions in Fig. 1, defined according to geographical criteria, and consistently with previous analysis (Gómez-Navarro et al., 2013), are comparatively large in their spatial extent. Indeed, they often include very different climatic characteristics, where the model produces opposite biases (see Figs. 4 to 8 in Gómez-Navarro et al., 2013).

CPD
11, 307–343, 2015

Further, the mean value could be potentially discard valuable information, such as regional deviations or widening of the distributions of temperature of precipitation within a region in different periods of time. To account for this important piece of climatic variability, Figs. 2 and 3 show the time series of the interdecile range of the spatial distribution of the seasonal means of grid-cell temperature and precipitation within each region. This provides information beyond the mean value alone, enabling also the evaluation of the evolution of the spatial variability of climate within regions.

Low frequent variability in the median generally translates to variability in the decile, i.e. the distributions shift in time as a whole, with little changes in their shape. This indicates that the median is a valid indicator for the regional evolution of all percentiles. This relation holds less well for precipitation, especially in summer and to a larger degree in the reconstruction. This is potentially due to the convective and localized character of summer precipitation (Gómez-Navarro et al., 2014).

The median series in Figs. 2 and 3 already suggest that differences between the Maunder (1645–1715) and Dalton (1790–1830) minima and the recent 20th century climatology (1961–1990) disagree between the simulation and reconstructions. However, while the percentiles reflect changes in the mean temperature, shifts in the distributions are rather small in the order of 1 to 2 °C colder means and quartiles. Most notable is the cooling for both periods in the winter SCA temperature. Distinct precipitation changes occur only for SCA and only in winter, with low solar forcing periods being drier than the recent climatology (see Fig. 3).

The underlying temperature PDFs generally agree well between the simulation and the reconstruction, in contrast to the evolution of the median time-series. Simulated winter temperature distributions are close or similar for IBE, SCA, BRI, TUR and ALP. Simulated summer temperature distributions are clearly biased towards a colder mean in all regions. Nevertheless the shape of the distributions is generally similar (not shown).

The simulation and reconstruction disagree more on the PDFs of winter and summer precipitation. The differences between the Maunder Minimum, the Dalton Minimum and the late 20th century climatology are spatially less homogeneous across regions. Gen-

CPD
11, 307–343, 2015

erally, the mean is underestimated and the extremes are overestimated for southern European winter precipitation, while summers are generally less dry in those regions in the simulation. On the other hand northern Europe shows the opposite for both seasons.

4 Dynamical consistency of simulation and reconstructions

The available gridded reconstructions of winter and summer temperatures, precipitation and sea level pressure allow not only to evaluate the temporal evolution at certain locations, but also to analyse the spatial structures of dominant modes of variability. Moreoever their evolution in different periods and the relation between modes of different variables can be investigated with canonical correlations. With the latter approach we gain insight in the dynamical consistency among reconstructions and between reconstructions and the simulation.

4.1 Modes of variability for SAT and precipitation

Figure 4 shows the first EOF for winter (left) and summer (right) SAT for the CRU data set (top row), MM5-ECHO-G (middle) and the Luterbacher et al. (2004, 2007) reconstructions (bottom row). The patterns are based on observations for the 1901–1990 period, whereas for the model and the reconstructions they are calculated for the period 1501–1990. The time period used to calculate the EOFs appears to be of minor relevance. Indeed, the patterns are robust, exhibiting only minor changes when the 1901–1990 period is used in the simulation and reconstructions (see discussion below). The second and third EOFs, also representing a remarkable amount of variance, are discussed here just briefly and shown in the supplementary material. Note that the maps are not normalised, but they contain the corresponding units for each variable, so the spatial integral of the square of the pattern is proportional to the variance explained by the respective pattern. In order to facilitate the comparison, the same color scale

CPD
11, 307–343, 2015

is used in all maps. Therefore the patterns are multiplied by different scaling factors, indicated in the top right corner of each panel (Fig. 4).

Reconstruction and the simulation agree well on the shape of the main EOF pattern of winter and summer SAT variability. They represent similar amounts of variability (indicated in each map), and also the total variance is similar. Note, for example, that the scaling factors consistently vary among datasets, and that summer maps had to be multiplied by a larger factor, indicating that summer series show less variability, as already pointed out by (Gómez-Navarro et al., 2013) and discussed in the former section. Although here only the leading variability mode is shown, this general conclusion applies also to the higher indexed EOFs (see supplementary material). The simulation, coherently with the observations, exhibits a monopole pattern centred over Eastern Europe, whereas this centre is slightly shifted towards the Baltic Sea in the reconstruction in both seasons. The resemblance between observations and reconstructions increases when the 1901–1990 period alone is considered (not shown), resulting in the slight sensitivity of the pattern to the choice of period. Note that a resemblance between the CRU data and the reconstructions, especially when the same period is used for the calculation, could be expected. This is so due to the fact that the reconstruction is calibrated against observations and the reconstructions are bound by PCA-regression to show very similar EOF patterns through the whole period (Raible et al., 2006). In the simulation, there is a larger agreement between 20th century and the full-period EOFs (not shown), suggesting that the main patterns of variability are not very sensitive to their respective base period, and more importantly, that the arguably short length of observation records appears to be adequate to calibrate the proxy data.

The simulated and reconstruction SAT, tend to attribute more variance to the first EOF in winter (71 and 72 % of total variance in the model and reconstructions, respectively) compared to observations (61 %). This difference is stronger in summer, when the leading mode in the observations represents 36 % of the total variance compared to 57 and 48 % in the model and reconstructions, respectively. This indicates that the simulated temperature covariance matrix is too homogeneous, particularly in summer,

CPD
11, 307–343, 2015

which is a reminder of the limitations of climate simulations: the zonal circulation in the driving GCM is too strong. This leads to a circulation regime in the RCM that is reminiscent of that observed in winter. Regarding the reconstruction, the larger proportion of variance represented by the reconstruction's leading EOF highlights again that using a truncated EOF-basis in the PCA-regression results only in partial representation of the true variability. The second and third EOFs are broadly similar in the reconstructions and observations for summer temperature, although their order is inverted. They still show similar gradient-like patterns, with the direction of the greatest gradient slightly tilted in the simulation compared to that in the reconstructions and the observations, respectively.

Figure 5 is similar to Fig. 4 but for precipitation (higher order modes of variability are shown in the supplementary material). In winter all datasets agree well and show a strong North–South dipole with the node at about 55° N. This pattern highlights the well-known difference between the Mediterranean area and Northern Europe. However, although the spatial structure agrees, the first mode represents more variance in the reconstruction than in the observations. The simulated leading variability mode represents 34 % of the winter variance, compared to a very similar 30 % in the CRU dataset. However the difference is larger in the reconstruction, where this mode explains up to 46 % of the total variance. In summer the leading mode of variability represents just 15 % in the observations. This can be explained by the fact that the precipitation regime is less influenced by the large-scale circulation. Despite the too strong zonal driving global simulation, this is consistent with the regional simulation, where the leading EOF also represents a low percentage of variance (12 %). However this is in strong contrast to the reconstruction, where the first EOF alone is able to account for 40 % of total variance. For the summer season, the spatial pattern of the observed and the simulated precipitation agree relatively well, while the North–South gradient observed in these datasets is changed mostly to a strong pole over the Alpine region, with a slight gradient to the North-East. The clearly dominating first mode in the reconstructions shows that the reconstructed precipitation regime is too homogeneous.

CPD
11, 307–343, 2015

This conclusion matches similar findings obtained through Pseudoproxy Experiments (Gómez-Navarro et al., 2014), where it has been shown how the linear regression used in Pauling et al. (2006) tends to underestimate the spatial variability of precipitation.

In the following a brief description on how the main variability modes compare between the GCM and the RCM is given. This comparison allows to characterise when the downscaling adds value, and represents an aspect of the analysis not shown by (Gómez-Navarro et al., 2013). The main variability modes of SAT exhibit in both seasons very similar patterns in both models, although the GCM reproduces less spatial variability, associated to its coarser spatial resolution (not shown). The percentage of variability represented by the main mode is 72 % in winter, indistinguishable from the RCM (Fig. 4). In summer this percentage drops to 38 %, in better agreement with observations, although the spatial structure shows generally less resemblance with observations, with a lower Southwest–Northeast gradient. For precipitation, the GCM compares worse than the RCM with CRU. In winter, the GCM is able to reproduce the characteristic main variability mode dominated by a North–South gradient shown in other data sets (see left column in Fig. 5). However the imprint of orography that can be appreciated in the RCM does not stand out in the GCM, resulting in an excessively homogeneous pattern. In summer the situation becomes more challenging, since not only the spatial structure is not realistic, but also the main variability mode represents 26 % of variance, empathizing the problems of the GCM to reproduce summer precipitation. Thus, results indicate that main variability modes are similar in both simulations, resulting from the strong forcing provided by the GCM trough the boundaries of the domain. Still, the RCM is able to add regional details to the simulated fields. However, this depends on the variable and season. SAT is more strongly influenced by the driving conditions than precipitation, where the imprint of orography is more pronounced. This is especially clear in summer, where precipitation in the GCM is barely able to reproduce the observed patterns. These results agree with similar findings described in other RCM studies (Gómez-Navarro et al., 2011, 2014).

CPD
11, 307–343, 2015

4.2 Dynamical consistency between variables

Canonical Correlation analysis (CCA) provides insight in the interrelation between different variables. Comparing observed relationships with the corresponding simulated ones provides an assessment of the model skill. Evaluating these relationships in reconstructions of different variables gives an indication of the consistency among independent reconstructions (e.g. Luterbacher et al., 2010). Figure 6 shows the canonical pair of patterns of SLP and SAT, and of SLP and precipitation, with the largest canonical correlation, as simulated by the MM5-ECHO-G and their counterpart in the observational record in winter. Note that in summer the evolution of temperature and especially precipitation is only to a lesser extent driven by the large-scale circulation. This is reflected by small canonical correlations. Hence, CCA is more useful for the winter season, and therefore only results for this season are discussed in detail.

In the subsequent figures, the first two rows correspond to the SLP-SAT canonical pair, whereas the last two correspond to pairs of SLP and precipitation. Figure 6 shows the results for the observations and the simulation in the control period. Considering the first canonical pair of SLP and SAT (top row), the canonical correlation is 0.93 for the observations. The patterns represent 42 % of total variance for SLP and 53 % for SAT, respectively. The SLP resembles the NAO pattern and is related to a North–South gradient pattern in SAT. The physical explanation for this correlation is the well known relationship between NAO and European temperature: a more zonal circulation in the North of Europe advects oceanic warm and moist air eastwards, leading to a positive temperature and precipitation anomaly in Northern Europe (Luterbacher et al., 2010).

A similar SLP pattern and physical mechanism can be identified in the SLP-PRE pair (third column), with a correlation of 0.95. The results within the simulation are shown in rows 2 and 4 of Fig. 6. The SLP-PRE pair roughly resembles the SLP-SAT pair, although the zonal circulation is shifted southwards. Despite the fact that the zonal circulation supports the same physical relation between variables, in this case the canonical correlation is lower, (r = +0.75). The SAT pattern represents a large amount of vari-

CPD
11, 307–343, 2015

ance and indeed resembles the leading EOF (see Fig. 4). The leading canonical pair of SLP-PRE exhibits a centre of high pressures in the North Atlantic which reinforces the northwestern component of wind and is responsible for increasing precipitation in Western Europe, whereas it produces precipitation deficits in Norway and Turkey. This mechanism results in a strong link, producing a correlation of 0.91, although it explains a relatively small amount of winter variability (only 19 % in the simulation).

Figure 7 is similar to Fig. 6, but for the period 1750–1990 and for the reconstructions instead of observations. This is the period available for the SLP reconstruction. None of the patterns for the longer period resembles perfectly the pair in the observations (compare Figs. 6 and 7) indicating that relationships between variables are sensitive to the period used. There are two potential reasons for this lack of robustness: first, the strong forcing in the 20th century may influence the canonical pairs either due to the strong anthropogenic trend in the zonal circulation in the driving simulation or due to a strong trend-component in the temperature field. Second, we have to keep in mind the simplified covariance and the potentially reduced signal in the reconstruction. The simulated canonical pair of SLP-SAT has a canonical correlation of 0.79 whereas the correlation for the reconstruction is 0.28. Again, the canonical pairs appear to be dominated by the temperature variability. The leading pairs for reconstruction and simulation both show a temperature gradient from the South-West to the North-East which is dynamically related to a slight wave-like disturbance of the zonal flow and related changes in the advection of air masses. The reconstruction and the simulation disagree on the location and character of flow centres.

The first SLP-PRE pair in the simulation (fourth row in Fig. 7), corresponds to the second canonical pair over the 1948–1990 period in the observations (not shown). Note that the first two pairs derived from observations are very similar, especially with respect to canonical correlations but also considering the representation of variances. However, the second pair represents more SLP-variance than the first one. The separation between both pairs is more distinct in the longer period of analysis and in that case the ranking of the two leading pairs is exchanged. Hence we decided to show the

CPD
11, 307–343, 2015

third canonical pair for the reconstruction, which is the apparent dynamic equivalent to the simulated one but shows much smaller canonical correlations (0.12 in the reconstruction and 0.89 in the simulation) while representing broadly consistent amount of variance. The small correlation signals that dynamical relations between both patterns may be weak. Indeed we would expect the NAO-like SLP-pattern to relate an intensified zonal flow to a decrease of precipitation in Southern Europe, which is opposite to the pattern the reconstructed pair implies.

5 Discussion and conclusions

This study assesses the agreements and disagreements between a regional climate (high-resolution) simulation for Europe and reconstructions for SAT, precipitation and SLP from the 16th century to the 20 th century. Our analyses complements the work by Gómez-Navarro et al. (2013), who compared the same simulation to observations for the 20th century.

Results indicate biases in regional means, especially noteworthy for summer temperature and winter precipitation. The biases between the simulation and reconstructions are similar to those described when comparing the model with an observational dataset. In part they can be explained by an enhanced zonal circulation in the GCM simulation that is not substantially ameliorated by the RCM, rather than by deficiencies within the reconstructions. Although reconstructions and the simulation seem to correctly reproduce most of the spatio-temporal variability, there is little agreement in their temporal evolution. The mismatch in the temperature, especially in the last decades, can originate in the missing anthropogenic aerosol forcing in the simulation. Additionally, early instrumental time series can show warm biases caused by the lack of modern thermometer screens (Frank et al., 2007a, b). Although we do not necessarily expect the reconstructed and simulated temperature evolution to agree in the earlier periods due to the potentially dominant internal variability, we also acknowledge that the lack of stratospheric dynamics in both the regional and the global simulation may account

CPD
11, 307–343, 2015

for some disagreement. Specifically, a too low top atmospheric layer in the model and no ozone chemistry reduce the ability of the model to correctly represent the potential top-down influences of solar activity changes on the atmospheric circulation in the North Atlantic sector, e.g., the North Atlantic Oscillation and in turn European climate variability (Shindell et al., 2001; Anet et al., 2013). Finally, the simplifications carried out to implement the volcanic forcing simply through artificial variations (reductions) of the TSI (Gómez-Navarro et al., 2013) might be an additional source of errors that contributes to reduce the agreement between the simulation and reconstructions.

Obviously, the reconstructions also suffer from uncertainties, which have to be considered in addressing the reliability of the simulation by comparing to the proxy-based data sources. A prominent disagreement is the winter warming trend within the first half of the 18th century (Jones and Briffa, 2006), which stands out in the reconstructions but lacks in the simulation. This disagreement could be an indication of a too simplistic simulated climate, which is not able to produce extreme situations comparable to this event recorded in the reconstructions. Also internal variability could dominate the temporal evolution, effectively hiding the imprint of external forcing on the regional scale.

Internal variability, reconstruction uncertainty and potential shortcomings of the simulation in representing forced climate may also explain the disagreement in the magnitude of change between recent decades and the periods of the Maunder and Dalton minima. Again, the lack of 20th century anthropogenic aerosol forcing is likely the most important factor.

EOF and CCA analysis unveiled the lack of dynamic consistency between reconstructions and the weak explanatory power of dominant canonical pairs. Although this is not surprising, it highlights the qualitative character of reconstructions based on environmental and documentary proxies and the large uncertainties in our estimates about past climates. This further implies that we are unlikely about to understand past climate changes based on one data source alone. On the other hand, the plausibility of simulated dynamics has to be assessed through tests with proxy-based hypotheses.

CPD
11, 307–343, 2015

Other assessments of consistency among independent reconstructions have been carried out in the literature. Casty et al. (2007) employed gridded reconstructions of SAT, precipitation and Geopotential at 500 hPa to investigate combined patterns of climate variability over Europe for the 1766–2000 period. A prominent difference with the data sets employed in the present analysis is that the three reconstructions employed by Casty et al. (2007) use completely independent indicators, entirely based on instrumental data for each variable. This reduces the length of the reconstructions, but in turn ensures independence, which enabled the authors to evaluate the consistency between reconstructions though EOF analysis applied to the combined fields of the three variables. The authors reported similar NAO-like behaviour as that described herein for the observations and simulations, with the large-scale flow driving seasonal temperature and precipitation over Europe, especially in winter. They also analysed the co-variability between SAT and precipitation. This study carefully avoids stabilising such link, since the data sets used here are not fully independent (both SAT and precipitation reconstructions share some indications). However, the CCA approach adopted here allows studying the co-variability between SLP and the other two variables. The weaker and physically inconsistent link we identify, especially with respect to the Pauling et al. (2006) reconstructions, raises concerns about the reliability of these reconstructions.

Coordinated reconstruction efforts as, for instance, related to PAGES2k (PAGES 2k Consortium, 2013) will increase the number of available proxy records. This, in conjunction with newly developed reconstruction methods, is expected to provide more realistic uncertainty estimates of the spatial fields and spatially averaged reconstructions. In addition, proxy system models (e.g. Evans et al., 2013) will provide a better basis for proxy-model comparison as they enable a direct modelling of the proxy under consideration within the virtual world of a climate model. This may help to evaluate e.g. the stationarity of proxy-climate relationships and the different sources and degrees of uncertainty implicit in empirical reconstruction methods.

In conclusion, although regional climates are generally better represented by the RCM compared to the driving GCM (Gómez-Navarro et al., 2013), the downscaling

CPD
11, 307–343, 2015

is not able to compensate for biases in the driving circulation. This leads to biases in the comparison with the reconstructions that are clearly attributable to model deficiencies. However, we cannot describe simulated and reconstructed anomalies with respect to today's climate as generally inconsistent, although the temporal evolution is different enough to raise concerns over the ability of the simulation to produce extremely anomalous situations as those recorded by the reconstructions. Further, potentially dynamically inconsistent reconstructions prevent to address the reliability of forced changes in the dynamics. It remains an open question whether a lack of common forced signals is due to weak forcing effects relative to the internal variability of the climate system, due to erroneous representation of climate dynamics in the model or due to uncertainty in the reconstructions.

The Supplement related to this article is available online at doi:10.5194/cpd-11-307-2015-supplement.

Acknowledgements. This work was funded by the PRIME2 project (priority program INTERDYNAMIK, German Research Foundation) and the SPEQTRES project (Spanish Ministry of Economy and Competitiveness, ref. CGL2011-29672-C02-02). Juan José Gómez-Navarro thanks the funding provided by the Oeschger Centre for Climate Change Research and the Mobiliar lab for climate risks and natural hazards (Mobilab).

References

Andreae, M. O., Jones, C. D., and Cox, P. M.: Strong present-day aerosol cooling implies a hot future, Nature, 435, 1187–1190, doi:10.1038/nature03671, 2005. 313

Anet, J. G., Muthers, S., Rozanov, E., Raible, C. C., Peter, T., Stenke, A., Shapiro, A. I., Beer, J., Steinhilber, F., Brönnimann, S., Arfeuille, F., Brugnara, Y., and Schmutz, W.: Forcing of stratospheric chemistry and dynamics during the Dalton Minimum, Atmos. Chem. Phys., 13, 10951–10967, doi:10.5194/acp-13-10951-2013, 2013. 310, 329

CPD
11, 307–343, 2015

Anet, J. G., Muthers, S., Rozanov, E. V., Raible, C. C., Stenke, A., Shapiro, A. I., Brönnimann, S., Arfeuille, F., Brugnara, Y., Beer, J., Steinhilber, F., Schmutz, W., and Peter, T.: Impact of solar versus volcanic activity variations on tropospheric temperatures and precipitation during the Dalton Minimum, Clim. Past, 10, 921–938, doi:10.5194/cp-10-921-2014, 2014. 310

Booth, B. B. B., Dunstone, N. J., Halloran, P. R., Andrews, T., and Bellouin, N.: Aerosols implicated as a prime driver of twentieth-century North Atlantic climate variability, Nature, 484, 228–232, doi:10.1038/nature10946, 2012. 313

Casty, C., Raible, C. C., Stocker, T. F., Wanner, H., and Luterbacher, J.: A European pattern climatology 1766–2000, Climate Dynamics, 29, 791–805, doi:10.1007/s00382-007-0257-6, 2007. 330

Eden, J. M., Widmann, M., Maraun, D., and Vrac, M.: Comparison of GCM- and RCM-simulated precipitation following stochastic postprocessing, J. Geophys. Res. Atmos., 119, 11040–11053, doi:10.1002/2014JD021732, 2014. 310

Evans, M. N., Tolwinski-Ward, S. E., Thompson, D. M., and Anchukaitis, K. J.: Applications of proxy system modeling in high resolution paleoclimatology, Quaternary Sci. Rev., 76, 16–28, doi:10.1016/j.quascirev.2013.05.024, 2013. 309, 310, 330

Frank, D., Buntgen, U., Bohm, R., Maugeri, M., and Esper, J.: Warmer early instrumental measurements versus colder reconstructed temperatures: shooting at the moving target, Quaternary Sci. Rev., 26, 3298–3310, 2007a. 328

Frank, D., Esper, J., and Cook, E. R.: Adjustment for proxy number and coherence in large-scale temperature reconstruction, Geophys. Res. Lett., 34, L16709, doi:10.1129/2007GL030571, 2007b. 328

Franke, J., González-Rouco, J. F., Frank, D., and Graham, N. E.: 200 years of European temperature variability: insights from and tests of the proxy surrogate reconstruction analog method, Clim. Dynam., 37, 133–150, doi:10.1007/s00382-010-0802-6, 2010. 310

Franke, J., Frank, D., Raible, C. C., Esper, J., and Brönnimann, S.: Spectral biases in tree-ring climate proxies, Nature Climate Change, 3, 360–364, doi:10.1038/nclimate1816, 2013. 309

Gómez-Navarro, J. J. and Zorita, E.: Atmospheric annular modes in simulations over the past millennium: no long-term response to external forcing, Geophys. Res. Lett., 40, 3232–3236, doi:10.1002/grl.50628, 2013. 310, 313

Gómez-Navarro, J. J., Montávez, J. P., Jerez, S., Jiménez-Guerrero, P., Lorente-Plazas, R., González-Rouco, J. F., and Zorita, E.: A regional climate simulation over the Iberian Penin-

CPD
11, 307–343, 2015

sula for the last millennium, Clim. Past, 7, 451–472, doi:10.5194/cp-7-451-2011, 2011. 309, 310, 311, 325
Gómez-Navarro, J. J., Montávez, J. P., Jiménez-Guerrero, P., Jerez, S., Lorente-Plazas, R., González-Rouco, J. F., and Zorita, E.: Internal and external variability in regional simulations of the Iberian Peninsula climate over the last millennium, Clim. Past, 8, 25–36, doi:10.5194/cp-8-25-2012, 2012. 309, 315, 319
Gómez-Navarro, J. J., Montávez, J. P., Wagner, S., and Zorita, E.: A regional climate palaeosimulation for Europe in the period 1500–1990 – Part 1: Model validation, Clim. Past, 9, 1667–1682, doi:10.5194/cp-9-1667-2013, 2013. 309, 310, 311, 312, 315, 317, 318, 319, 320, 323, 325, 328, 329, 330
Gómez-Navarro, J. J., Werner, J., Wagner, S., Luterbacher, J., and Zorita, E.: Establishing the skill of climate field reconstruction techniques for precipitation with pseudoproxy experiments, Clim. Dynam., 1–19, doi:10.1007/s00382-014-2388-x, 2014. 314, 319, 321, 325
Goosse, H., Renssen, H., Timmermann, A., Bradley, R. S., and Mann, M. E.: Using paleoclimate proxy-data to select optimal realisations in an ensemble of simulations of the Clim. Past millennium, Clim. Dynam., 27, 165–184, doi:10.1007/s00382-006-0128-6, 2006. 310
Goosse, H., Guiot, J., Mann, M. E., Dubinkina, S., and Sallaz-Damaz, Y.: The medieval climate anomaly in Europe: comparison of the summer and annual mean signals in two reconstructions and in simulations with data assimilation, Global Planet. Change, 84–85, 35–47, doi:10.1016/j.gloplacha.2011.07.002, 2012. 310
Harris, I., Jones, P., Osborn, T., and Lister, D.: Updated high-resolution grids of monthly climatic observations – the CRU TS3.10 Dataset, Int. J. Climatol., 34, 623–642, doi:10.1002/joc.3711, 2014. 313
Jones, P. D. and Briffa, K. R.: Unusual Climate in Northwest Europe During the Period 1730 to 1745 Based on Instrumental and Documentary Data, Climatic Change, 79, 361–379, doi:10.1007/s10584-006-9078-6, 2006. 318, 329
Kalnay, E., Kanamitsu, M., Kistler, R., Collins, W., Deaven, D., Gandin, L., Iredell, M., Saha, S., White, G., Woollen, J., Zhu, Y., Leetmaa, A., Reynolds, R., Chelliah, M., Ebisuzaki, W., Higgins, W., Janowiak, J., Mo, K. C., Ropelewski, C., Wang, J., Jenne, R., and Joseph, D.: The NCEP/NCAR 40-year reanalysis project, B. Am. Meteorol. Soc., 77, 437–471, 1996. 313
Kim, J.-W., Chang, J.-T., Baker, N. L., Wilks, D. S., and Gates, W. L.: The Statistical Problem of Climate Inversion: determination of the Relationship between Lo-

CPD
11, 307–343, 2015

cal and Large-Scale Climate, Mon. Weather Rev., 112, 2069–2077, doi:10.1175/1520-0493(1984)112<2069:TSPOCI>2.0.CO;2, 1984. 310

Küttel, M., Xoplaki, E., Gallego, D., Luterbacher, J., García-Herrera, R., Allan, R., Barriendos, M., Jones, P. D., Wheeler, D., and Wanner, H.: The importance of ship log data: reconstructing North Atlantic, European and Mediterranean sea level pressure fields back to 1750, Clim. Dynam., 34, 1115–1128, doi:10.1007/s00382-009-0577-9, 2010. 315

Luterbacher, J., Xoplaki, E., Dietrich, D., Rickli, R., Jacobeit, J., Beck, C., Gyalistras, D., Schmutz, C., and Wanner, H.: Reconstruction of sea level pressure fields over the Eastern North Atlantic and Europe back to 1500, Clim. Dynam., 18, 545–561, doi:10.1007/s00382-001-0196-6, 2002. 314

Luterbacher, J., Dietrich, D., Xoplaki, E., Grosjean, M., and H., W.: European sesonal and annual temperature variability, trends and extremes since 1500, Science, 303, 1499–1503, 2004. 314, 315, 317, 322, 338

Luterbacher, J., Liniger, M. A., Menzel, A., Estrella, N., Della-Marta, P. M., Pfister, C., Rutishauser, T., and Xoplaki, E.: Exceptional European warmth of autumn 2006 and winter 2007: historical context, the underlying dynamics, and its phenological impacts, Geophys. Res. Lett., 34, L12704, doi:10.1029/2007GL029951, 2007. 314, 315, 317, 322, 338

Luterbacher, J., Koenig, S. J., Franke, J., van der Schrier, G., Zorita, E., Moberg, A., Jacobeit, J., Della-Marta, P. M., Küttel, M., Xoplaki, E., Wheeler, D., Rutishauser, T., Stössel, M., Wanner, H., Brázdil, R., Dobrovolný, P., Camuffo, D., Bertolin, C., van Engelen, A., Gonzalez-Rouco, F. J., Wilson, R., Pfister, C., Limanówka, D., Nordli, Ø., Leijonhufvud, L., Söderberg, J., Allan, R., Barriendos, M., Glaser, R., Riemann, D., Hao, Z., and Zerefos, C. S.: Circulation dynamics and its influence on European and Mediterranean January–April climate over the past half millennium: results and insights from instrumental data, documentary evidence and coupled climate models, Climatic Change, 101, 201–234, doi:10.1007/s10584-009-9782-0, 2010. 310, 326

PAGES 2k Consortium: Continental-scale temperature variability during the past two millennia, Nat. Geosci., 6, 339–346, doi:10.1038/ngeo1797, 2013. 330

Pauling, A., Luterbacher, J., Casty, C., and Wanner, H.: Five hundred years of gridded high-resolution precipitation reconstructions over Europe and the connection to large-scale circulation, Clim. Dynam. , 26, 387–405, doi:10.1007/s00382-005-0090-8, 2006. 314, 315, 325, 330, 339

CPD
11, 307–343, 2015

Phipps, S. J., McGregor, H. V., Gergis, J., Gallant, A. J. E., Neukom, R., Stevenson, S., Ackerley, D., Brown, J. R., Fischer, M. J., and van Ommen, T. D.: Paleoclimate Data–Model Comparison and the Role of Climate Forcings over the Past 1500 Years*, J. Climate, 26, 6915–6936, doi:10.1175/JCLI-D-12-00108.1, 2013. 310

Raible, C. C., Casty, C., Luterbacher, J., Pauling, A., Esper, J., Frank, D. C., Büntgen, U., Roesch, A. C., Tschuck, P., Wild, M., Vidale, P.-L., Schär, C., and Wanner, H.: Climate variability-observations, reconstructions, and model simulations for the Atlantic-European and Alpine region from 1500–2100 AD, Climatic Change, 79, 9–29, doi:10.1007/978-1-4020-5714-4_2, 2006. 323

Raible, C. C., Lehner, F., González-Rouco, J. F., and Fernández-Donado, L.: Changing correlation structures of the Northern Hemisphere atmospheric circulation from 1000 to 2100 AD, Clim. Past, 10, 537–550, doi:10.5194/cp-10-537-2014, 2014. 310

Schimanke, S., Meier, H. E. M., Kjellström, E., Strandberg, G., and Hordoir, R.: The climate in the Baltic Sea region during the last millennium simulated with a regional climate model, Clim. Past, 8, 1419–1433, doi:10.5194/cp-8-1419-2012, 2012. 311

Shindell, D. T., Schmidt, G. A., Mann, M. E., Rind, D., and Waple, A.: Solar forcing of regional climate change during the Maunder Minimum, Science, 294, 2149–2152, doi:10.1126/science.1064363, 2001. 310, 329

Schmidt, G. A., Annan, J. D., Bartlein, P. J., Cook, B. I., Guilyardi, E., Hargreaves, J. C., Harrison, S. P., Kageyama, M., LeGrande, A. N., Konecky, B., Lovejoy, S., Mann, M. E., Masson-Delmotte, V., Risi, C., Thompson, D., Timmermann, A., Tremblay, L.-B., and Yiou, P.: Using palaeo-climate comparisons to constrain future projections in CMIP5, Clim. Past, 10, 221–250, doi:10.5194/cp-10-221-2014, 2014. 309

Tingley, M. P., Craigmile, P. F., Haran, M., Li, B., Mannshardt, E., and Rajaratnam, B.: Piecing together the past: statistical insights into paleoclimatic reconstructions, Quaternary Sci. Rev., 35, 1–22, doi:10.1016/j.quascirev.2012.01.012, 2012. 309

von Storch, H. and Zwiers, F.: Statistical Analysis in Climate Research, Cambridge University Press, 2007. 316

Wagner, S., Fast, I., and Kaspar, F.: Comparison of 20th century and pre-industrial climate over South America in regional model simulations, Clim. Past, 8, 1599–1620, doi:10.5194/cp-8-1599-2012, 2012. 310

Wetter, O., Pfister, C., Luterbacher, J., Werner, J., Siegfried, W., Glaser, R., Riemann, D., Himmelsbach, I., Contino, A., Burmeister, K., Litzenburger, L., Barriendos, M., Brazdil, R., Kiss,

CPD
11, 307–343, 2015

A., Camenisch, C., Limanowka, D., Pribyl, K., Labbé, T., Retsö, D., Bieber, U., Rohr, C., Spring, J., Nordli, O., Soderberg, J., and Alcoforado, M.: The year-long unprecedented European heat and drought of 1540 – a worst case scenario, Climatic Change, 125, 349–363, 2014. 319

Widmann, M., Goosse, H., van der Schrier, G., Schnur, R., and Barkmeijer, J.: Using data assimilation to study extratropical Northern Hemisphere climate over the last millennium, Clim. Past, 6, 627–644, doi:10.5194/cp-6-627-2010, 2010. 310

Yoshimori, M., Stocker, T. F., Raible, C. C., and Renold, M.: Externally forced and internal variability in ensemble climate simulations of the Maunder Minimum, J. Climate, 18, 4253–4270, doi:10.1175/JCLI3537.1, 2005. 310

Zanchettin, D., Timmreck, C., Graf, H.-F., Rubino, A., Lorenz, S., Lohmann, K., Krüger, K., and Jungclaus, J. H.: Bi-decadal variability excited in the coupled ocean–atmosphere system by strong tropical volcanic eruptions, Clim. Dynam., 39, 419–444, doi:10.1007/s00382-011-1167-1, 2012. 310

Zorita, E., Moberg, A., Leijonhufvud, L., Wilson, R., Brázdil, R., Dobrovolný, P., Luterbacher, J., Böhm, R., Pfister, C., Glaser, R., Söderberg, J., and González-Rouco, F.: European temperature records of the past five centuries based on documentary information compared to climate simulations, Climatic Change, 101, 143–168, doi:10.1007/s10584-010-9824-7, 2010. 318

CPD
11, 307–343, 2015

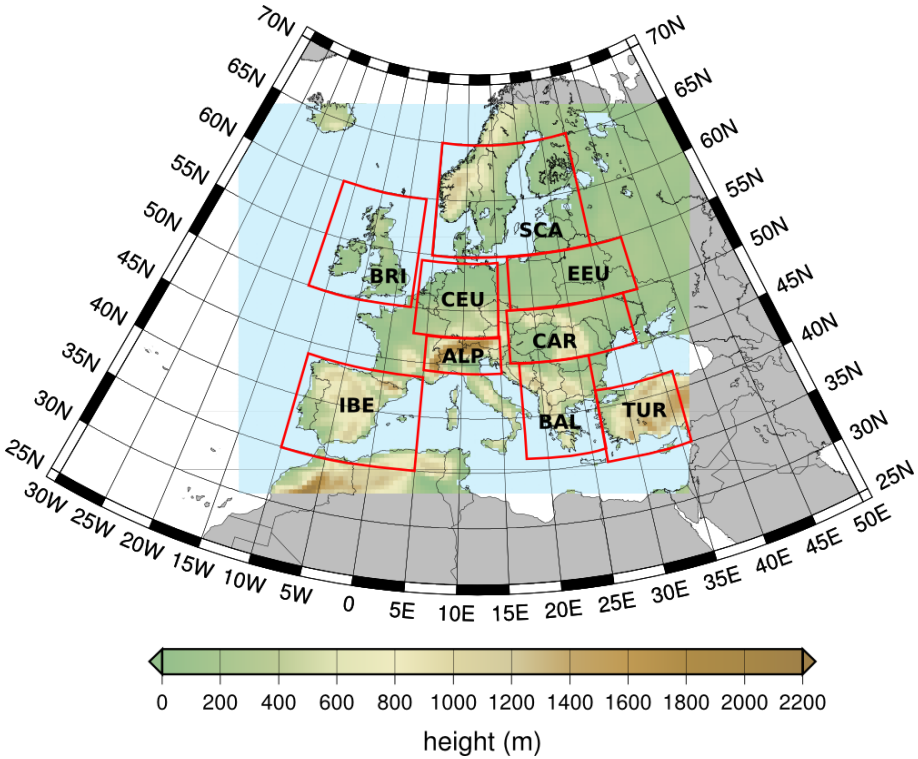

Figure 1. Topography and landmask implemented in the regional simulation, with a horizontal resolution of 45 km. The rectangles show the nine subregions used for more detailed analysis. IBE, Iberian Peninsula; BRI, British Isles; CEU, Central Europe; EEU, Eastern Europe; SCA, Scandinavian Peninsula and Baltex Sea; CAR, Carpathian Region; BAL, Balkan Peninsula; ALP, Alps; TUR, Turkey.

CPD
11, 307–343, 2015

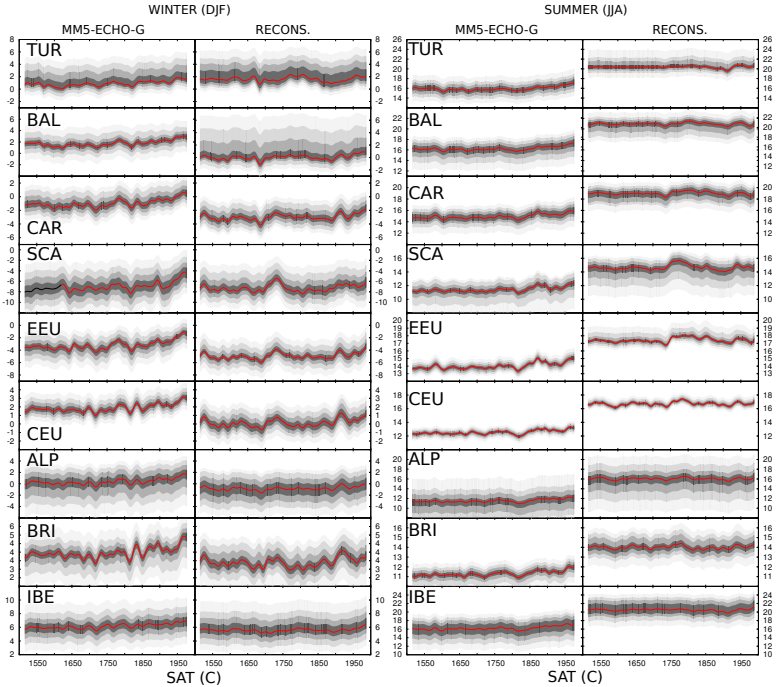

Figure 2. Temporal series of SAT in the nine areas indicated in Fig. 1 for the winter (columns 1 and 2) and summer (columns 3 and 4) in the MM5-ECHO-G simulation and the Luterbacher et al. (2004, 2007) temperature reconstructions. The thick red lines represent the median, whereas different levels of shaded gray indicate the decile ranges (40–60, 30–70, 20–80 and 10–90, respectively). After the calculation of the deciles, all series are smoothed through a Hamming window of 31 time steps to emphasise the low-frequency variability. To facilitate the comparison, the scale is the same between the simulation and the reconstruction, although it is different for each area and season, reflecting the different mean values and variances among different subregions.

CPD
11, 307–343, 2015

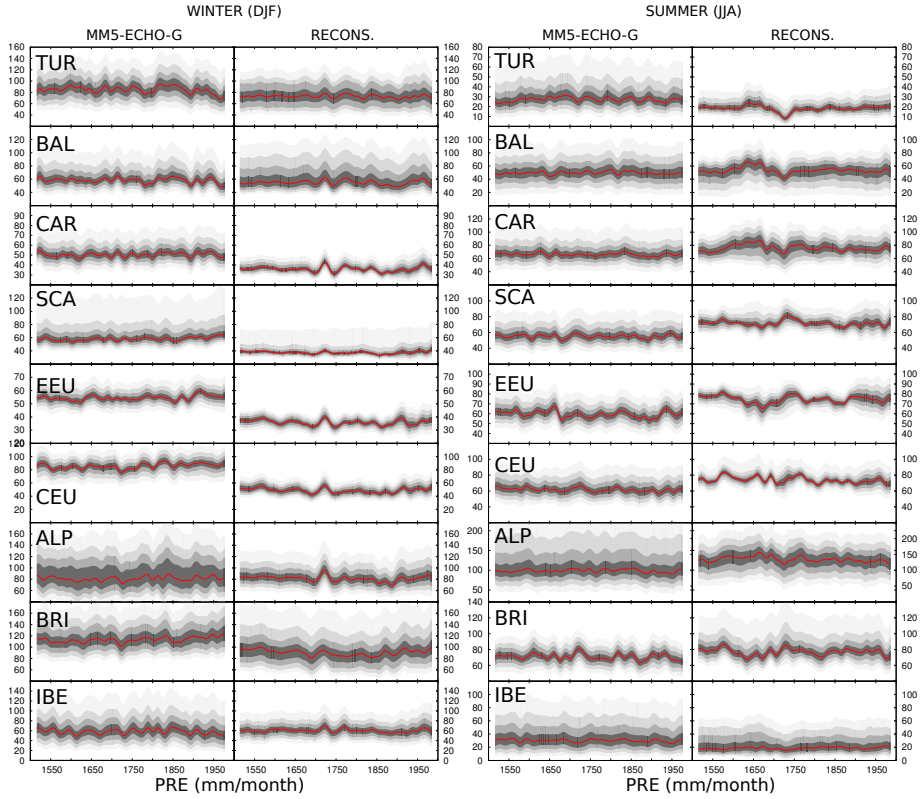

Figure 3. As Fig. 2 but for simulated precipitation and the Pauling et al. (2006) reconstructions. Note the different scaling of the *y* axes.

CPD
11, 307–343, 2015

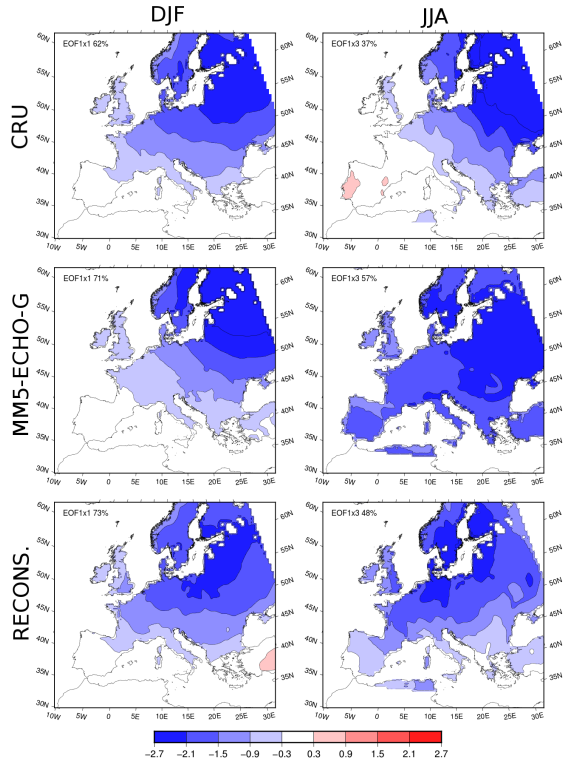

Figure 4. First EOF of winter (left) and summer (right) SAT. Each row depicts the results for the CRU dataset (top), the MM5-ECHO-G simulation (middle) and the reconstructions (bottom). For the first case the 1901–1990 period is employed, whereas for the other the period 1501–1990 is considered. Note that the patterns carry the units of the variable, and thus they are proportional to the squared root of the variance that each pattern represents. Hence, and to facilitate the comparison, each pattern has been multiplied by a scaling factor, indicated in the top right corner of the figure. The percentage of total variance represented by each pattern is also indicated. The units are ˚C.

CPD
11, 307–343, 2015

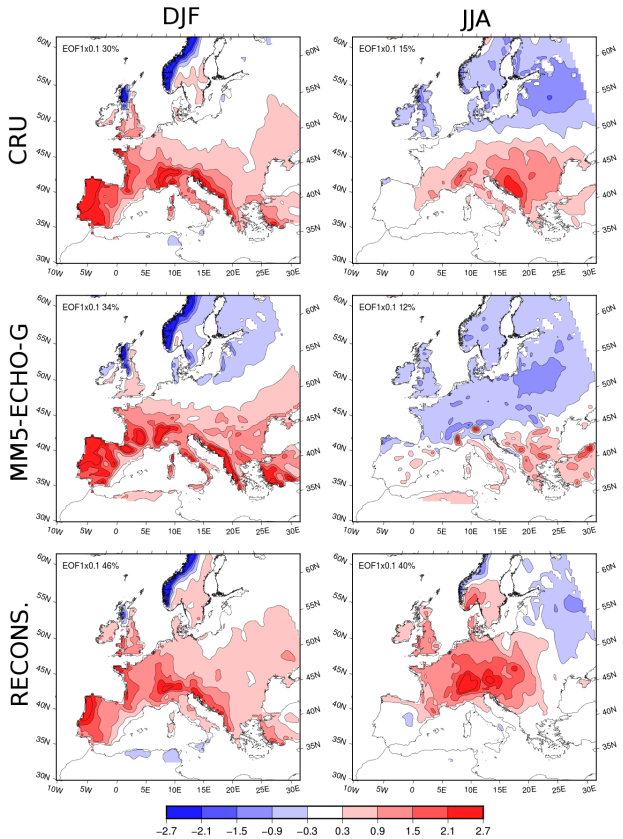

Figure 5. As Fig. 4 but for precipitation. The units are mm month^{-1}.

CPD
11, 307–343, 2015

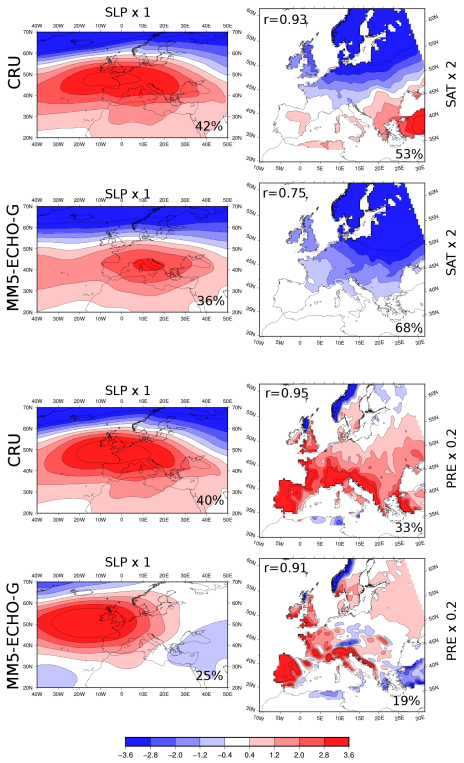

Figure 6. Canonical correlation pattern pairs of SLP and SAT (rows 1 and 2), and SLP and precipitation (rows 3 and 4) in winter. Each figures depicts the percentage of variance explained by each pattern and the canonical correlation associated with the pair. The results are calculated in the observational record (rows 1 and 3) and in the MM5-ECHO-G dataset (rows 2 and 4) during the period 1901–1990. Note that the SLP has been obtained directly from the driving GCM, since the window of interest lies outside the RCM domain. As in Figs. 4 and 5, the patterns have been multiplied by a scaling factor that allows using the same color scale in every map. The SAT units are ˚C, SLP is shown in Pa, whereas precipitation units are mm month^{-1}.

CPD
11, 307–343, 2015

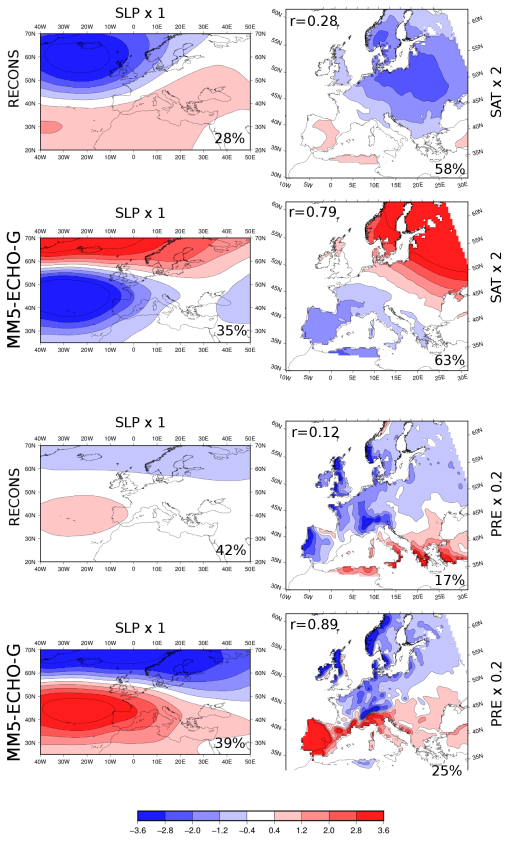

Figure 7. As in Fig. 6 but for the simulation and reconstructions. The calculations are based on the overlap period of the simulation and the SLP reconstructions, 1750–1990.

CPD
11, 307–343, 2015